ACS APPLIED MATERIALS & INTERFACES

Research Article

www.acsami.org

Low Surface Energy Plane Exposed Co_3O_4 Nanocubes Supported on Nitrogen-Doped Graphene as an Electrocatalyst for Efficient Water Oxidation

Santosh K. Singh,[†,‡] Vishal M. Dhavale,[†,‡] and Sreekumar Kurungot*[,†,‡]

[†]Physical and Materials Chemistry Division, CSIR-National Chemical Laboratory, Dr. Homi Bhabha Road, Pune 411 008, India

[‡]Academy of Scientific and Innovative Research, Anusandhan Bhawan, 2 Rafi Marg, New Delhi 110 001, India

Supporting Information

ABSTRACT: Herein, we report a simple and scalable synthesis of Co_3O_4 nanocubes possessing exposed low surface energy planes supported on nitrogen-doped graphene (Co_3O_4-NC/NGr) by a hydrothermal method as an efficient electrocatalyst for water oxidation. Three different types of morphologies of Co_3O_4 (i.e., nanocubes, blunt edge nanocubes and spherical particles) have been synthesized by systematically varying the reaction time. Subsequently, their catalytic activity toward oxygen evolution reaction (OER) has been screened in alkaline medium. Among the three different morphologies, the intermediate architecture (i.e., the blunt edged nanocubes designated as Co_3O_4-NC/NGr-12h) has shown the highest OER activity. The catalyst displayed an overpotential (η) of ~280 mV at 10 mA/cm^2 in 1 M KOH solution, which is lower than that of the other prepared samples such as Co_3O_4-NC/NGr-3h (~348 mV), Co_3O_4-NC/NGr-9h (~356 mV), Co_3O_4-NC/NGr-24h (~320 mV), Co_3O_4-NC/Gr-12h (~300 mV) and Co_3O_4 (~310 mV). Along with that, the electrochemical stability of the catalyst is also found to be remarkably good. The role of the low index planes of Co_3O_4 nanocubes (Co_3O_4-NC) and the importance of the doped nitrogen in the carbon framework for the uniform dispersion and direct coupling with Co_3O_4-NC have been examined. The controlled interplay of the exposed crystal planes of Co_3O_4 and its dispersion and synergistic interaction with the nitrogen-doped graphene are found to be the decisive factors in bringing in the modulated OER activity of the system.

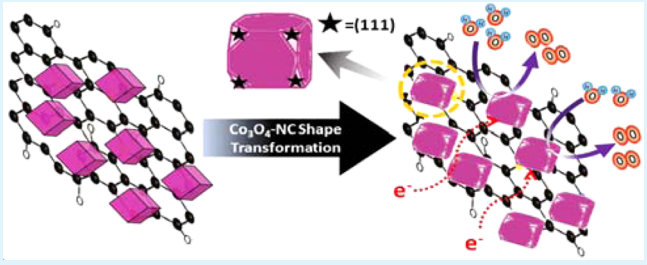

KEYWORDS: *water oxidation, low index planes, nanocubes, electrocatalyst*

INTRODUCTION

Oxygen evolution reaction (OER) is gaining generous attention due to its widespread applicability in the field of green and clean energy technologies such as rechargeable metal−air batteries, electrolysis cells and solar-to-fuel production. However, the overall efficiency of these systems is decided by the performance of the oxygen evolution electrocatalyst.[1−3] Mainly, the efficiency for the conversion of solar-to-fuel is greatly constrained by higher anodic overpotential of oxygen evolution reaction (OER).[2] Contemporary OER catalysts based on rare earth metals, such as RuO_2, IrO_2 and their combinations with other metals, may not be economically viable due to their high cost and scarcity.[4] To overcome these issues, nonprecious multimetallic electrocatalysts,[5,6] metal oxides[3,7] and anisotropic structures of M-Co[8,9] (M = Ni, Fe, Mn, Zn, etc.) have been explored for OER. However, these catalysts fail to deliver better activity and stability all the while keeping the overpotential in an acceptably low range.[5,6,8,9] Along with this, the dispersion of such kinds of materials on a highly conducting support is another issue that needs to be tackled effectively. This put forth a challenging demand in front of the concerned scientific community for developing new electrocatalysts having redefined activity characteristics.

There are extensive research activities on the metal oxide based materials as electrocatalysts, including nickel,[5,6,10] iron,[3,7] cobalt based oxides/hydroxides,[1,2,3,7] spinels and perovskites,[11,12] reported in the literature. An important outcome of some of these studies is the identification of the fact that the exposed crystal planes of these metals play a major role in reducing the overpotential involved in OER.[13] The peculiar morphological structures of metals and their oxides like cube, flower-like, octahedron, rod structures, etc. have attracted wide attention in the field of electrochemical device applications.[13−15] Along with that, the chemistry of diverse energy facets and difference in the binding properties of the intermediates and/or products with such facets are additional determining factors in deciding the overall catalytic activity of the materials under operating conditions.

Received: September 20, 2014
Accepted: December 12, 2014
Published: December 12, 2014

DOI: 10.1021/am506450c
ACS Appl. Mater. Interfaces 2015, 7, 442−451

In addition, recently, various carbon allotropes (graphene, carbon nanotubes (CNTs), carbon nanofibers (CNFs), fullerene, etc.) have been explored as OER electrocatalysts.[16,17] Along with this, various nitrogen-doped carbon allotropes also have been reported for OER. However, the activity depends on the level of doping up to a certain limit.[17,18] The performance of the carbon materials alone as a catalyst is relatively low compared to the metal oxide-supported counterparts.[19−21] Conversely, these materials have been validated as good catalyst supports rather than as catalysts due to their high mechanical strength, excellent electrical conductivity and chemical stability.[22−25] Therefore, synthesis of engineered nanostructures of metal oxide dispersed on a highly conducting substrate (like, graphene nanostructures, heteroatom-doped graphene or CNTs) will be an elegant solution over the currently used RuO_2 and IrO_2 based electrocatalysts.[22,23,26,62,66] Among the reported metal oxide supported on carbon allotropes, the Co oxide based catalysts have exhibited better activity toward the energy storage and conversion devices.[8,9,26] The observed activity is mainly because of easy and effective electron transfer between the mixed valancies of Co oxide by hopping process, which facilitate the efficient water oxidation.[27,28] Recently, Wu et al.[29] reported that the Co_3O_4 particles supported on single-walled CNTs could show better activity in terms of an overpotential of 370 mV at 66 A/g in 1 M KOH solution compared to the unsupported Co_3O_4 nanocrystals. Moreover, Dai et al.[22] have testified that the Co_3O_4 nanocrystals grown on reduced graphene oxide exhibited an overpotential of ∼320 mV at 10 mA/cm^2 in 1 M KOH solution. The aforementioned reports also reveal that the direct nucleation, growth and anchoring of Co oxide nanocrystals with appropriate support are determining factors in deciding the activity characteristics of the catalysts. Along with these, the exposed crystal facets of the metal oxides are expected to play a major role in controlling the overpotential for the reaction. Even though these relations are broadly discussed in different contexts, the present literatures do not highlight the importance of geometry and definite energy facets which majorly contributes during OER. Therefore, a concerted effort to correlate the aforementioned contributing factors is necessary to get clear insights on the nature of the active centers required for facilitating OER at reduced overpotentials.

From the above discussion, it can be seen that the right morphology of the Co_3O_4 nanostructures along with their homogeneous dispersion on a conducting carbon substrate are the two essential criteria to be met in the path for realizing a high performance, cost-effective OER catalyst with significantly reduced overpotential. Taking advantage of the intrinsic properties of the structures and their planes, we tried to develop a nitrogen-doped graphene (NGr) supported blunt edged Co_3O_4 nanocube (Co_3O_4-NC) electrocatalyst having more number of low index exposed planes displaying comparable activity and stability as that of the reported state-of-the-art catalysts for water oxidation.[22,23,30] The intimate contact and synergetic coupling effect between Co_3O_4-NC and nitrogen of NGr provided the significantly higher activity and stability toward OER.

EXPERIMENTAL SECTION

Materials. Cobalt acetate, graphite, phosphoric acid (H_3PO_4), potassium hydroxide (KOH), sulfuric acid (H_2SO_4), potassium permanganate ($KMnO_4$), hydrazine hydrate ($N_2H_4{\cdot}H_2O$) and melamine were procured from Sigma-Aldrich. Hydrogen peroxide (H_2O_2), hydrochloric acid (HCl) and ethanol were procured from Thomas Baker. All the chemicals were used as such without any further purification.

Synthesis of Graphene Oxide (GO). Improved Hummer's method was used for the synthesis of GO.[31,32] In brief, 3 g of graphite was well mixed with the required amount of $KMnO_4$. The above mixture was slowly added into a mixture of H_3PO_4:H_2SO_4 (1:9). After the complete addition, the reaction mixture was kept under stirring at 60 °C for 24 h. Later, the obtained reaction mixture was poured into ice cooled water containing 3% H_2O_2. A yellow precipitate was obtained that was separated by centrifugation at 10000 rpm, and was subsequently washed well with copious deionized (DI) water, followed by 30% HCl, to remove the unwanted impurities. Finally, the wet cake was washed with ethanol and acetone, and allowed to dry at room temperature.

Synthesis of Reduced Graphene Oxide (Gr). GO was reduced by aqueous solution of hydrazine hydrate.[19] Briefly, 50 mg of GO was dispersed in 50 mL of DI water and the mixture was kept under vigorous magnetic stirring for 30 min. 20 μL of hydrazine hydrate solution was added into the above mixture under stirring for 12 h at 80 °C. Finally, the reaction mixture was centrifuged at 10000 rpm, washed with DI water and dried at 80 °C in an oven for 10 h.

Synthesis of Nitrogen-Doped Graphene (NGr). A mixture of GO (1 g) and melamine (5 g) was dispersed in DI water (100 mL) by sonication (10 min), followed by magnetic stirring for 24 h. Subsequently, the mixture was dried under magnetic stirring at 80 °C. The obtained melamine−GO solid powder was heated at about 800 °C in an argon atmosphere for about 4 h. After that, the furnace was cooled down to room temperature under inert atmosphere. Thus, obtained black colored powder was termed as NGr. This was used as the substrate material for synthesizing the Co_3O_4-NC/NGr catalysts.[33,34]

Synthesis of Co_3O_4-NC/NGr and Co_3O_4-NC/Gr Catalysts. *Synthesis of Co_3O_4-NC/NGr Catalysts.* Cobalt acetate (60 mg) and NGr (40 mg) were dispersed in an ethanol−water (3:2) mixture and the mixture was ultrasonicated for 30 min by using a probe sonicator. The well dispersed mixture was transferred into a 50 mL Teflon coated stainless steel autoclave and was kept at different time intervals (3, 9, 12 and 24 h) at 120 °C. The obtained products were filtered and washed with DI water to remove the unreacted metal salts. Finally, the materials were dried in an oven at 80 °C for 10 h. The samples prepared by maintaining the time intervals of 3, 9, 12 and 24 h are designated as Co_3O_4-NC/NGr-3h, Co_3O_4-NC/NGr-9h, Co_3O_4-NC/NGr-12h and Co_3O_4-NC/NGr-24h, respectively.

Synthesis of Co_3O_4-NC/Gr. Cobalt acetate (60 mg) and Gr (40 mg) were dispersed in an ethanol−water (3:2) mixture, and the mixture was ultrasonicated for 30 min by using a probe sonicator. The well dispersed mixture was transferred into a 50 mL Teflon coated stainless steel autoclave and was kept at 120 °C for 12 h. The obtained product was filtered and washed with DI water to remove the unreacted metal salts. The obtained product is named as Co_3O_4-NC/Gr-12h.

CHARACTERIZATION

For the high resolution transmission electron microscopy (HR-TEM) analysis, the samples were prepared by sonicating 1 mg of the catalyst in 5 mL of isopropyl alcohol and drop-coating on a carbon coated 200 mesh Cu grids. Moreover, the catalyst drop coated Cu grid was dried under an IR lamp and the sample thus prepared was used for the imaging purpose. The TEM images were obtained by using an FEI, TECNAI G2 F20 instrument operated at an accelerated voltage of 300 kV (Cs = 0.6 mm, resolution 1.7 Å). X-ray diffraction (XRD) patterns were recorded on PANalytical instrument using Cu $K\alpha$ radiation (λ = 1.54 Å) at a scanning rate of 2° min^{-1} and a step size of 0.02° in 2θ. Thermogravimetric analysis (TGA) was performed on a SDTQ600 TG-DTA analyzer. TGA analyses have been performed under oxygen environment with 10 °C/min temperature ramp. X-ray photoelectron spectroscopy

DOI: 10.1021/am506450c
ACS Appl. Mater. Interfaces 2015, 7, 442−451

(XPS) was carried out on a VG Microtech Multilab ESCA 3000 spectrometer that was equipped with an Mg Kα X-ray source ($h\nu$ = 1.2536 keV). An HR 800 Raman spectrometer (Jobin Yvon, Horiba, France) was used for Raman analysis of all the samples using a 632 nm red laser (NRS 1500 W).

Electrochemical Characterization. A VMP-3 model Bio-Logic potentiostat was used to investigate the electrochemical analysis by cyclic voltammetry (CV), linear sweep voltammetry (LSV) and rotating ring disc electrode (RRDE) (Pine Instruments) in a conventional three-electrode test cell with glassy carbon as the working electrode, Hg/HgO as the reference electrode and a platinum flag as the counter electrode. Current has been normalized by diving with geometrical surface area of the electrode. For preparing the working electrode, the glassy carbon (GC) electrode was polished with 0.3 and 0.05 μm alumina slurries, and then a 10 μL aliquot of the catalyst slurry made by sonicating 5 mg of the catalyst in 1 mL of 3:2 ethanol–water mixtures was drop-coated on the electrode surface. Subsequently, 2 μL of 0.01 wt % Fumion diluted with ethanol was applied on the whole surface of the electrode to yield a uniform thin film, which was subsequently dried in air and was used as the working electrode for all electrochemical studies. An aqueous solution of 1 M KOH was used as the electrolyte for normal CV, RDE and RRDE studies. The potentials were normalized with respect to the reversible hydrogen electrode (RHE). All the electrochemical data were corrected with 65% iR compensation.

RESULTS AND DISCUSSION

Scheme 1 represents the hydrothermal methodology adopted for achieving the in situ dispersion of the blunt edged Co_3O_4 nanocubes on highly conducting two-dimensional (2-D) NGr (Co_3O_4-NC/NGr). The morphology of the Co_3O_4 has been confirmed through the transmission electron microscopy study. Figure 1a,b,j,k displays a well demarcated dispersion of Co_3O_4

Scheme 1. Schematic Illustration of the Synthesis of Co_3O_4 Nanocubes/NGr (Co_3O_4-NC/NGr) Electrocatalyst and Transformation of Cubical Structure to the Blunt Edge

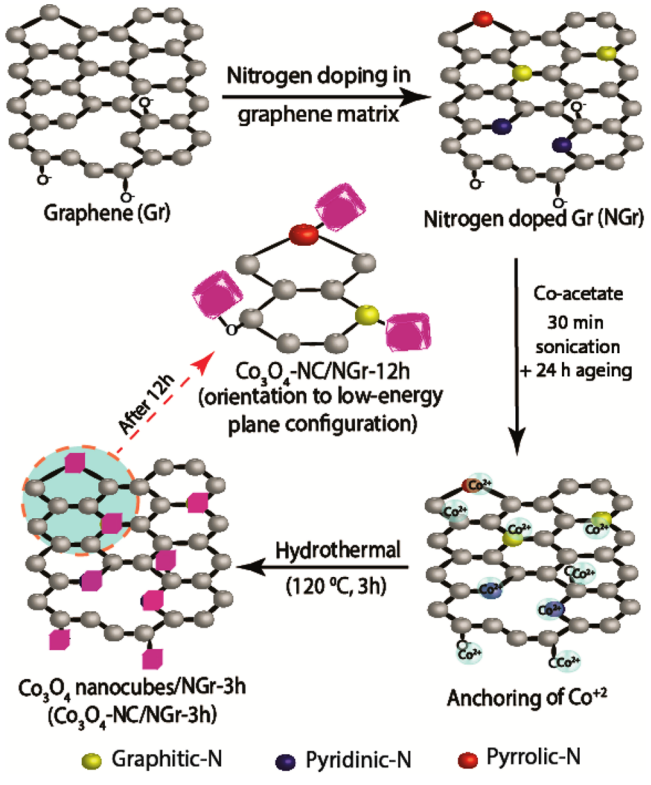

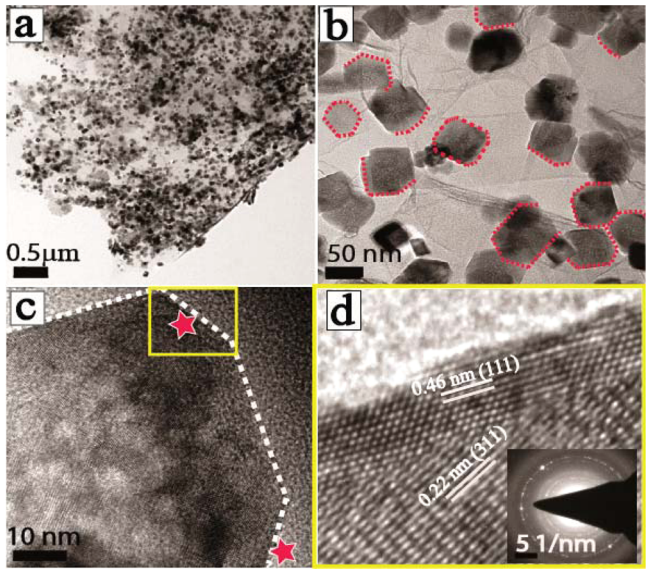

Figure 1. TEM images of Co_3O_4–NC/NGr-12h: (a) well dispersion of Co_3O_4–NC on NGr; (b) Co_3O_4-NC/NGr-12h with blunted edged Co_3O_4-NC, the blunt edges are marked with dotted red line; (c) high magnified TEM image of Co_3O_4-NC/NGr-12h, the red stars indicate the blunt edges and (d) exposed area of panel c marked with yellow color, which highlights the *d*-spacing values (inset is SAED pattern).

nanocubes (Co_3O_4-NC) on NGr with an average size of 50 ± 3 nm. However, the dispersion of Co_3O_4 on Gr, as can be seen in Figure 2a, is found to be poor compared to that on NGr. An apparent difference in the dispersion characteristics of Co_3O_4-NC on Gr in its doped and undoped states portraits a case of decisive role played by nitrogen as a dopant in creating a fertile substrate surface for facilitating the dispersion of the metal oxide nanoparticles. The better dispersion of Co_3O_4-NC on NGr is mainly credited to the interaction of nitrogen of NGr with Co_3O_4-NC.[24] Along with the influence of the nitrogen, the oxygen functional groups also are expected to play an influential role for maintaining the dispersion. Valid evidence on the existence of the interaction between NGr and Co oxide has been obtained by XPS, which is explained later in this paper.

The particle size histogram, which is presented in Figure S1 (Supporting Information), provides supplementary evidence on the importance of nitrogen doping for ensuring the controlled growth and size distribution of Co_3O_4-NC on NGr. The histogram suggests that the particle size distribution among the samples follows the order of Co_3O_4-NC/NGr-3h (~25 ± 3 nm) < Co_3O_4-NC/NGr-9h (~40 ± 3 nm) < Co_3O_4-NC/NGr-12h (~50 ± 3 nm) < Co_3O_4-NC/NGr-24h (~60 ± 3 nm). Compared to the NGr based systems, the Co_3O_4 dispersion on the system based on the undoped graphene (Co_3O_4-NC/Gr-12h) is found to be inhomogeneous with a broad particle size distribution (~50–80 ± 3 nm). Moreover, the size of Co_3O_4-NC supported on NGr is found to be increased from 25 to 60 nm, when the reaction time increased from 3 to 24 h, as shown in Figures 2m,n and S1 (Supporting Information). However, as can be seen in a later section, the amount of Co_3O_4 nanoparticles dispersed on NGr is also found to be varying

DOI: 10.1021/am506450c
ACS Appl. Mater. Interfaces 2015, 7, 442–451

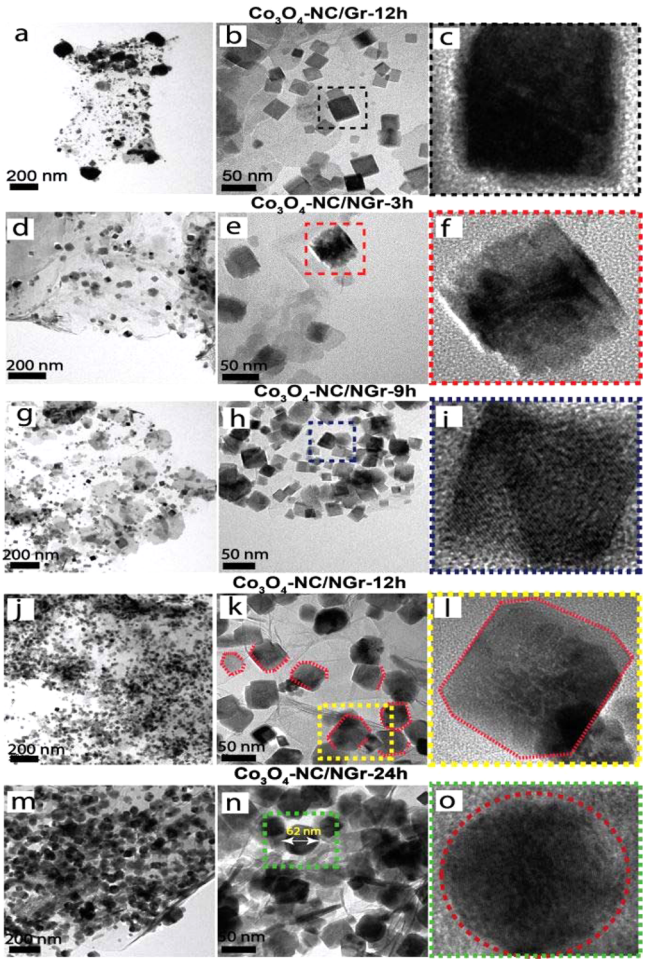

Figure 2. TEM images of Co_3O_4-NC/Gr-12h and Co_3O_4-NC/NGr electrocatalysts prepared at different time intervals (a and b) showing the dispersion of Co_3O_4 nanocubes supported on Gr. (c) Magnified portion of Co_3O_4-NC/Gr-12h in panel b marked with the black colored dash box. (d–i) TEM and HR-TEM images of Co_3O_4-NC/NGr-3h and Co_3O_4-NC/NGr-9h electrocatalysts showing dispersion of Co_3O_4-NC on NGr. (j–l) TEM and HR-TEM images of Co_3O_4-NC/NGr-12h. The blunt edged nanocubes are marked with dotted red colored lines. (m–o) TEM and HR-TEM images of Co_3O_4-NC/NGr-24h, showing spherical Co_3O_4 particles and the agglomeration of Co_3O_4 particles.

with the reaction time, where a shorter time duration such as 3 or 9 h is found to be insufficient to facilitate complete dispersion of the oxide particles on the substrate. Thus, the discrepancy in the size of Co_3O_4 nanoparticles can be partially originated by the differences in the accommodated particles by the NGr surface. Mainly, the large discrepancy in terms of the size of Co oxide between Co_3O_4-NC/NGr-12h and Co_3O_4-NC/Gr-12h, which are prepared under exactly identical experimental conditions, highlights the substantial role played by the doped nitrogen of NGr in establishing good dispersion characteristics of the oxide nanoparticles.

More importantly, with increase in the reaction time, the edges of Co_3O_4-NC are found to be started blunting prior to the agglomeration (Figure 1b,c). This could be attributed to the propensity of the crystal structure to undergo transformation of the higher surface energy planes into a low surface energy plane during the crystal growth.[13,20,21] Among the prepared samples, Co_3O_4-NC/NGr-12h has shown the existence of a low surface energy plane (blunt edge), which is marked in Figure 1c,d. The calculated *d*-spacing values of the blunt edged Co_3O_4-NC/NGr-12h planes are found to be 0.46 and 0.22 nm, which are attributed to the (111) and (311) planes of Co_3O_4-NC.[35,36] The crystallinity of the particles has been further confirmed through the selected area electron diffraction (SAED) pattern, which is shown as an inset in Figure 1d. Furthermore, as the reaction time increases to 24 h, the blunt edged cubes get converted into nearly spherical particles with an average size of 60 ± 3 nm. This transformation might be conceived due to the overgrowth of Co_3O_4 crystals at longer reaction times (Figure 2m,n).

Mainly, the surface energies (γ) of the low index crystallographic facets are in the order of $\gamma(111) < \gamma(100) < \gamma(110)$ for the face-centered cubic (fcc) crystal structures.[13,19−21] As mentioned above, at lower time duration of the reaction, the (111) planes are lying inside the perfect cube of Co_3O_4-NC (Figure S2, Supporting Information) and, hence, those planes are unable to be directly involve in the electrocatalytic reactions. However, as the time of the reaction increases, the corners of Co_3O_4-NC start to become blunt and thus expose the embedded and newly generated low index planes (Figures 1 and 2). Furthermore, to understand the exposure of the low index plane during structural transformations as triggered by the reaction conditions, we have carried out XRD analysis (Figure 3). The characteristic peaks of the well-defined spinel

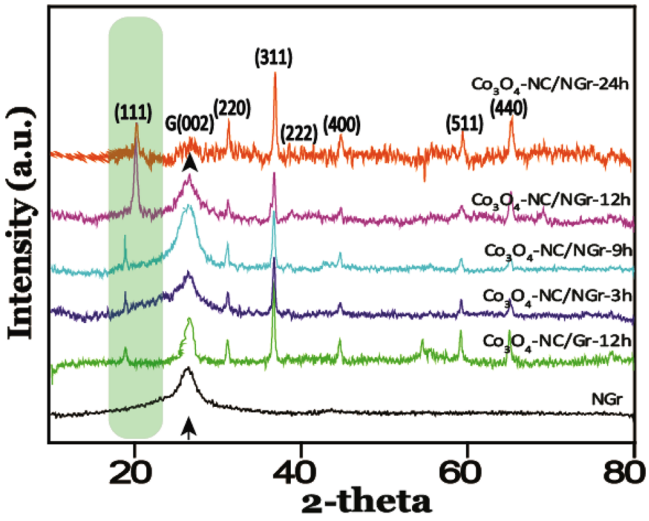

Figure 3. Comparative X-ray diffraction patterns of NGr, Co_3O_4-NC/Gr-12h and Co_3O_4-NC/NGr-X h (X = 3, 9, 12 and 24 h). The arrow represents the graphitic (002) plane of NGr.

Co_3O_4-NC are appearing at 2θ values of 19.85, 31.20, 36.65, 38.90, 42.14, 59.51 and 65.28°, which correspond to the (111), (220), (311), (222), (400), (511) and (440) planes of the Co_3O_4 phase,[37] respectively. Moreover, the peak at ∼26.39° corresponds to the graphitic (002) plane of NGr. The obtained diffraction peaks, thus, clearly highlight that the supported cobalt oxide is a normal spinel.[37] On increasing the reaction time, however, it can be seen from the figure that the relative intensity of the (111) plane progressively increases up to the 12 h, which stands out as valid evidence of gradual exposure of the low index crystal plane under the hydrothermal conditions (a schematic illustration for the exposure of the (111) plane is provided in Figure S2, Supporting Information). In a stark contrast to this trend, the (111) peak intensity is found to be

DOI: 10.1021/am506450c
ACS Appl. Mater. Interfaces 2015, 7, 442−451

decreased in the case of Co_3O_4-NC/NGr-24h (Figure 3). This could be correlated to the transformation of the shape of Co_3O_4 particles from cubical to spherical as evident from the TEM images, which is substantiated by the relatively higher intensity of the (311) plane in the XRD diffraction pattern.[63,64] The observations related to the planes and shapes of Co_3O_4-NC from the XRD data clearly validate the results obtained from the HR-TEM analysis.

The amount of Co_3O_4 loading with respect to the reaction time has been confirmed through the thermogravimetric analysis (TGA) (Figure S3, Supporting Information) under oxygen atmosphere. The TGA profiles in all the cases display a sudden weight loss after 500 °C corresponding to the degradation of carbon. However, looking at it very closely, the carbon degradation in the case of Co_3O_4-NC supported on Gr and NGr has been observed at a lower temperature compare to that of NGr alone. This could account for the easy degradation/oxidation of carbon in the presence of the metal oxide.[38,39] The residue obtained subsequent to the degradation of the carbon gives an estimation of the dispersed Co_3O_4 in each sample. Among the nitrogen-doped systems, the Co_3O_4 loading has been found to be following the order of Co_3O_4-NC/NGr-3h (~12.60 wt %) < Co_3O_4-NC/NGr-9h (~19.30 wt %) < Co_3O_4-NC/NGr-12h (~26.40 wt %) < Co_3O_4-NC/NGr-24 h (~35.00 wt %). The Co_3O_4 content on Co_3O_4-NC/Gr-12h is estimated to be ~23.20 wt %, which is slightly lower than that obtained on Co_3O_4-NC/NGr-12h, even though both the samples are prepared under identical conditions. The higher loading of Co_3O_4 on NGr can be credited to the presence of extra anchoring and nucleating sites on doped graphene and favorable interaction between the Co_3O_4 and NGr, as nitrogen doping is well-known as an intercalation that can bring in nano-order dislocations and electron density changes in the graphitic framework.[40,41]

The change in the properties, including the local and chemical configuration, has been examined through X-ray photoelectron spectroscopy (XPS) analysis. XPS analysis of NGr shows the presence of C 1s, O 1s, N 1s and Co 2p without intervention by any impurities. Deconvoluted XPS spectra of C 1s of NGr (Figure S4, Supporting Information) show four different peaks at 284.58, 286.97, 288.49 and 290.16 eV, which are corresponding to the −C═C−, −C—O, −C═O and −O—C═O, respectively.[16] The N 1s spectrum of NGr has been deconvoluted by fitting the spectra with three sub peaks at 398.61 (pyridinic-N), 400.48 (pyrrolic-N) and 402.84 eV (quaternary-N).[42] Moreover, the lower binding energy shift (~1.2 eV) of the N 1s spectrum of Co_3O_4-NC/NGr-12h (397.2 eV), compared to N 1s of NGr (398.61 eV) stands out as credible evidence of the effective interaction between Co_3O_4-NC and nitrogen of NGr (shown in Figure 4c,d). This interaction might be established via the electron transfer between the Co oxide and NGr, leading to an apparent change in the binding energy of the N 1s spectrum. This is also validated from the difference in the electronegativity values between N and Co, where the Pauling electronegativity values are 3.0 for N and 1.8 for Co. As N is more electronegative, electron density will be transferred from Co to N, which results into a shift in the binding energy of N 1s.[43,44] It has been reported that the interaction of Co/Fe ions with nitrogen of porphyrins leads to a lower binding energy shift of nitrogen.[43,44] Furthermore, the nitrogen percentage is found to be almost the same (i.e., 3.8 wt %) in the cases of NGr (Figure 4c) and Co_3O_4-NC/NGr-12h (Figure 4d), because the same batch

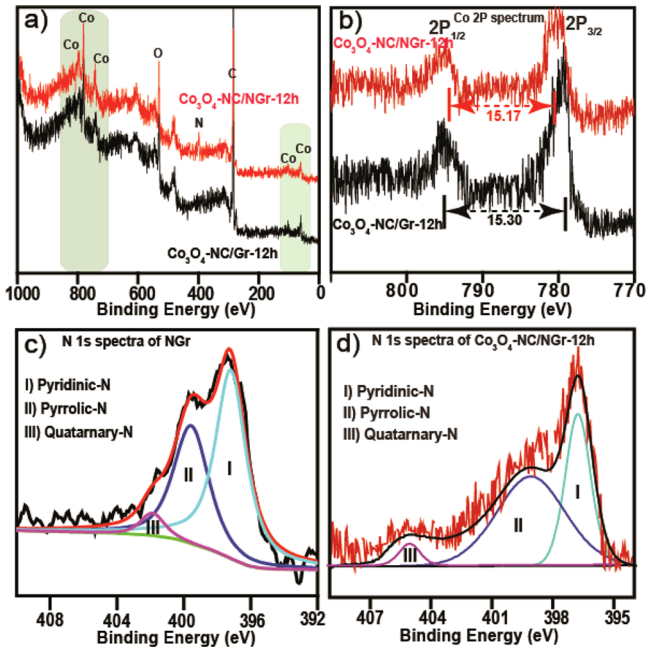

Figure 4. (a) Comparative XPS survey scan of Co_3O_4-NC/Gr-12h and Co_3O_4-NC/NGr-12h, (b) comparative Co 2p spectrum of Co_3O_4-NC/Gr-12h and Co_3O_4-NC/NGr-12h, (c) deconvoluted N 1s spectra of NGr and (d) deconvoluted N 1s spectra of Co_3O_4-NC/NGr-12h.

of NGr was used for the synthesis of all the Co_3O_4-NC supported NGr catalysts. Moreover, Figure 4a,b shows the Co 2p spectra, where the Co $2p_{3/2}$ (780.5 eV) and $2p_{1/2}$ (795.8 eV) peaks show the characteristic peak difference of ~16 eV.[45,46] Moreover, the slight shift in the binding energy of Co 2p of Co_3O_4-NC/NGr-12h compared to Co_3O_4-NC/Gr-12h could be attributed to the transfer of electron between nitrogen of NGr and Co oxide, which, eventually, leads to strong electronic interaction between Co_3O_4-NC and the doped nitrogen of NGr.

The mutual transfer of electron between the Co oxide and nitrogen of NGr has also been confirmed by Raman analysis. Figure 5 depicts the comparative Raman spectra for Gr, NGr, Co_3O_4-NC/Gr-12h and Co_3O_4-NC/NGr-12h. The Raman spectra present the typical features of the carbon materials at ~1327 and ~1589 cm^{-1}, which could be assigned to the defective and graphitic nature of the carbon.[42] Along with this, the Co_3O_4-NC supported Gr/NGr samples show additional cobalt oxide peak in the range of 150−750 cm^{-1}, which could be due to the transverse and longitudinal optical phonon mode vibrations of Co oxide.[47] Mainly, the G-band at 1589 cm^{-1} corresponds to the "in-plane" displacement of carbon atoms strongly coupled in the hexagonal sheets. This represents an ideal graphitic lattice vibration mode with E_2g symmetry, and thereby characterizes the highly ordered graphite carbon materials. The D-band (or "defect" band) at 1327 cm^{-1} is the characteristic of the disordered graphite and corresponds to a graphitic lattice vibration mode with A1g symmetry.[18,48] The intensity ratio of D- and G-band (I_D/I_G) is an index of the degree of disorder in the matrix and gives information on the average size of the sp^2 domains. The I_D/I_G ratio is found to be increased slightly from 1.32 to 1.47 for Gr and NGr, respectively, thereby providing evidence that the graphene structure is essentially defected upon the nitrogen doping.[13,33,34] However, the I_D/I_G ratio slightly decreases to 1.24

DOI: 10.1021/am506450c
ACS Appl. Mater. Interfaces 2015, 7, 442−451

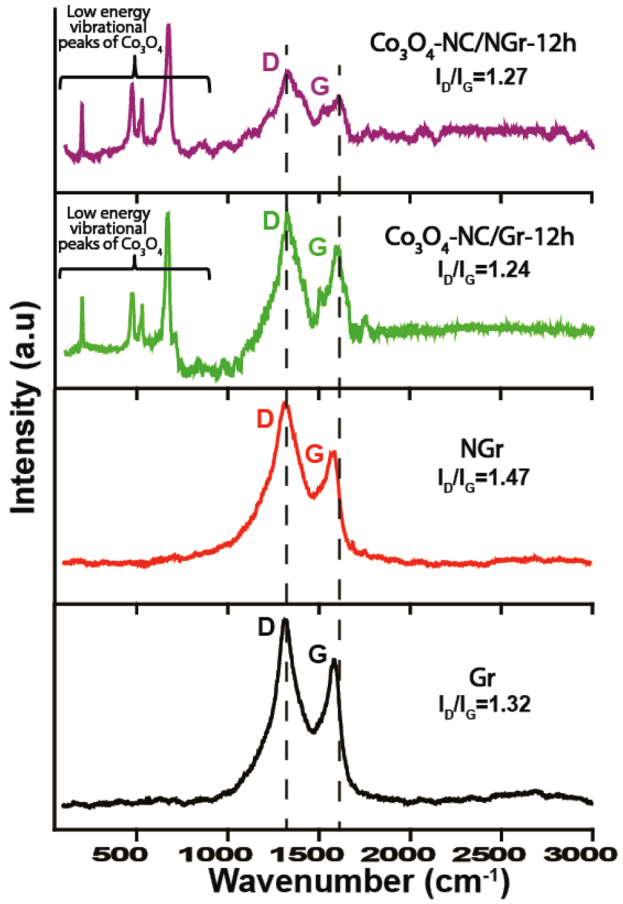

Figure 5. Comparative Raman spectra of Gr, NGr, Co_3O_4-NC/Gr-12h and Co_3O_4-NC/NGr-12h samples.

and 1.27 for Co_3O_4-NC/Gr-12h and Co_3O_4-NC/NGr-12h, respectively, thereby providing evidence that the graphene structure is restored up to some extent upon loading of Co_3O_4.[38,39] This also is associated with a significant shift of the G-band position for Co_3O_4-NC supported on Gr and NGr compared to their individual states. The obtained results are tabulated in Table S1 (Supporting Information).

The exposure of the low index crystal planes in Co_3O_4-NC and the synergistic electronic interactions between the nitrogen of NGr and the oxide moiety, as detailed in the previous sections, is expected to bring in modulated activity characteristics of the system toward OER. Hence, the effect of change in the electronic configuration and exposure of the low surface energy planes have been investigated by probing the OER activity of the systems by using 1 M KOH as the electrolyte. As mentioned earlier, the catalyst coated glassy carbon was used as the working electrode and Hg/HgO was employed as the reference electrode. The internal resistance was determined by impedance spectroscopy and the value is found to be ~15 Ω (Figure S5, Supporting Information). The potentials were reported with an iR compensation of 65%. An iR corrected comparative plot of the LSVs corresponding to OER is given in Figure 6a in which the onset potential for Co_3O_4-NC/Gr-12h and Co_3O_4-NC/NGr-12h has been observed to be 1.45 and 1.43 V, respectively. The OER profiles indicate that Co_3O_4-NC/NGr-3h and Co_3O_4-NC/NGr-9h give an overpotential of ~348 and ~356 mV, respectively, at 10 mA/cm^2, which is higher than that of Co_3O_4-NC/NGr-12h (~280 mV). The activity of the prepared catalyst has been separated with their

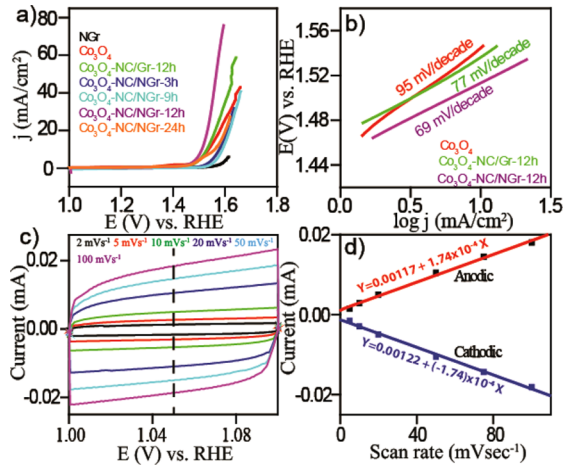

Figure 6. (a) Comparative LSV plots for NGr, Co_3O_4, Co_3O_4-NC/Gr-12h, Co_3O_4-NC/NGr-3h, Co_3O_4-NC/NGr-9h Co_3O_4-NC/NGr-12h and Co_3O_4-NC/NGr-24h in an nitrogen saturated 1 M KOH solution, with a scan rate of 10 mV/s. (b) Comparative Tafel plots of Co_3O_4-NC, Co_3O_4-NC/Gr-12h, Co_3O_4-NC/NGr-12h. (c) Capacitive CV of Co_3O_4-NC/NGr-12h recorded with different scan rates, where no apparent faradaic process has taken place. CV is performed in nitrogen saturated 1 M KOH; electrode geometrical area: 0.07065 cm^2. (d) Cathodic and anodic current vs scan rate plot at 1.05 V, and the calculated ESCA is found to be 6.44 cm^2.

individual components (i.e., NGr and Co_3O_4) (shown in Figure S7, Supporting Information) and it seems that the role of Co_3O_4 is more dominating over NGr. Co_3O_4 is appeared to be showing higher mass activity (43.06 mA $mg_{-Co_3O_4}^{-1}$) than NGr (5.15 $mAmg_{-NGr}^{-1}$), but their individual activities are much lower than the case when these two moieties are supported together (shown in Table S4, Supporting Information). It could be concluded that Co_3O_4 supported NGr samples show better mass activity compared to their individual entities, whereas Co_3O_4-NC/NGr-24h possesses lower activity due to the spherical morphology of Co_3O_4.

The significant improvement on the overpotential by 80−90 mV in the case of Co_3O_4-NC/NGr-12h clearly discloses the important role played by the exposed low index crystal planes (blunt edge) on the Co_3O_4 nanocubes and proper electronic contact with NGr for facilitating OER activity with low overpotential. The obtained overpotential value in the case of Co_3O_4-NC/NGr-12h is better (i.e., more negative) compared to the available literature results of the Co based catalysts (Table S2, Supporting Information)[49] and the state-of-the-art Ir/Ru oxide catalysts (Table S3, Supporting Information). This could be mainly attributed to the exposure of the (111) planes of the blunt edged cubes, which is a low surface energy plane with a better OH^- adsorption−desorption capacity.[8,9,50,51] Moving ahead in the catalyst series, a significantly higher overpotential has been observed with Co_3O_4-NC/NGr-24h (~320 mV) compared to that of Co_3O_4-NC/NGr-12h, even though the value is slightly lower than those of Co_3O_4-NC/NGr-3h and Co_3O_4-NC/NGr-9h. This further substantiates the critical role of the exposed low index crystal plane, as Co_3O_4-NC/NGr-24h has displayed mixed facets compare to Co_3O_4-NC/NGr-12h due to the extensive disintegration of the edges of the initially formed oxide nanocubes at the longer reaction duration.

With special focus on Co_3O_4-NC/NGr-12h, owing to its enhanced activity characteristics toward OER, we have tried to

DOI: 10.1021/am506450c
ACS Appl. Mater. Interfaces 2015, 7, 442−451

further explore the activity modulation accomplished by the system due to the structural and electronic changes. Figure S6 (Supporting Information) shows the cyclic voltammogram (CV) of Co_3O_4-NC/NGr-12h in a potential window of 0.9 to 1.7 V (vs RHE). This shows well defined redox peaks of cobalt oxide at 1.41 V (vs RHE) in the forward sweep, which is assigned to the formation of CoO_2, and at 1.36 V in the reverse sweep, due to the formation of CoOOH, along with the peak corresponding to oxygen evolution at ~1.5 V (vs RHE). The kinetics involved in the adsorption and desorption of the reactants and products during the OER has been investigated by analyzing the Tafel slopes (Figure 6b). The Tafel slope of Co_3O_4-NC/NGr-12h (~69 mV/decade) is found to be lower than those of Co_3O_4-NC/Gr-12h (95 mV/decade) and Co_3O_4 (~77 mV/decade). The lower Tafel slope in the former case highlights involvement of better kinetics and feasible mechanism during OER in alkaline medium. The lower Tafel slope of Co_3O_4-NC/NGr-12h is desirable to drive a large catalytic current density at low overpotential.[52,53] In the experiment, however, a deviation from the linear dependence of the logarithmic current density at high overpotentials has been observed, which is attributed to the strong influence by the evolved oxygen bubbles which limit the available surface area for the mass transport. Mainly, the current density of OER (i.e., the kinetics) is expected to be proportional to the catalytically active surface area.[53,54] Hence, the electrocatalytic active surface area (ECSA) of the material has been calculated by calculating the capacitance of the double layer at the solid–liquid interface with cyclic voltammetry. The potential is scanned in a nonfaradaic potential window (i.e., 1.0 to 1.1 V) at varying scan rates. The obtained current is plotted against the scan rate at 1.05 V (vs RHE), which gives a straight line (Figure 6c,d). The slope of the line is assigned to the electrochemical double layer capacitance (C_{dl}).[2,54] Furthermore, the ratio of C_{dl} (1.74×10^{-4}) to the specific capacitance C_s (27 μF)[2] of the metal catalyst gives the ECSA, and is found to be ~6.44 cm^2. Consequently, the roughness factor (RF) is obtained by dividing ECSA with the geometrical surface area of the electrode (0.070 625 cm^2). The estimated value of RF is found to be 91.18 ± 3. The electrochemical surface area serves as an approximate guide for the surface roughness within an order-of-magnitude accuracy. The obtained ECSA and roughness factor in the case of Co_3O_4-NC/NGr-12h is very close to the values reported for the state-of-art catalysts.[2,55]

Furthermore, the survivability of Co_3O_4-NC/NGr-12h under the OER experimental conditions has been investigated by anodic potential cycling for 500 cycles (Figure 7a) and chronoamperometry (Figure 7b) for 12 h at an overpotential of ~280 mV. The LSVs taken before and after the cyclic stability test (Figure 7a) show only 20% increase of the overpotential (the overpotential increased from 280 to 350 mV) at the practical current density of 10 mA/cm^2, which is better as compared to that reported for the Co based OER catalysts. For a better understanding of the durability characteristics of the present system with that of the few reported ones, a comparison with the available literature data is presented in Table S2 (Supporting Information). From the chronoamperometric study (Figure 7b), it has been found that the current density of Co_3O_4-NC/NGr-12h shows better sustainability compared to Co_3O_4-NC/Gr-12h, which gives approval to the stability and activity of the NGr supported catalysts and role of the existing low energy planes of Co_3O_4-NC/NGr-12h. The presence of nitrogen is also found to

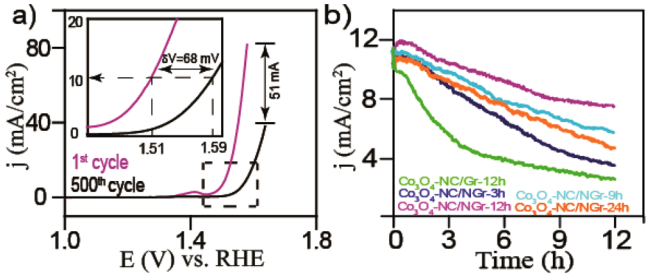

Figure 7. (a) Oxygen evolution curve of Co_3O_4–NC/NGr-12h catalyst before and after the 500 cycles stability performed in a potential window of 0.9 to 1.7 V (vs RHE) in a nitrogen saturated 1 M KOH solution with a scan rate of 10 mV/s and at 1600 rpm of the working electrode. Inset shows the change in potential at 10 mA/cm^2. (b) Comparative chronoamperometric stability of Co_3O_4-NC/Gr-12h, and Co_3O_4-NC/NGr-*x*h (x = 3, 9, 12, and 24) performed at an overpotential of 280 mV for 12 h.

increase the corrosion resistivity of the carbon support material by tuning the graphitization and modulating its intrinsic property.[17,38,39,42,56,57] The current density for Co_3O_4-NC/NGr-12h at the start of the experiment (i.e. t = 0) is 11.91 mA cm^{-2}, which falls to 8.21 mA cm^{-2} after 12 h (i.e., t = 12 h), a 31% decrease. The corresponding degradations in the cases of the other samples are 76, 58, 42 and 40% for Co_3O_4-NC/Gr-12h, Co_3O_4-NC/NGr-3h, Co_3O_4-NC/NGr-9h and Co_3O_4-NC/NGr-24h, respectively. Thus, the better activity and stability of Co_3O_4-NC/NGr-12h compared to the rest of the samples are attributed to the favorable contributions originated from the morphology, surface energy of the exposed low index planes (111) and the covalent interactions between Co_3O_4-NC and the nitrogen of NGr support (results are tabulated in Table S4, Supporting Information).[14] To understand the reason for the decrease in the performance, we have further characterized the material after the durability test. The TEM study shows that the structural integrity of Co_3O_4-NC/NGr-12h has been maintained after 500 potential cycling in a potential window of 1 to 1.7 V vs RHE (Figure S8a,b, Supporting Information). The size of Co_3O_4-NC is still around ~60 ± 5 nm. After the potential cycling, the aggregation of Co_3O_4-NCs was observed. This could be a reason for the decrease in the current and increase of the overpotential of the catalyst during OER. Along with this, the surface passivation also could affect the stability. Moreover, XPS was further employed to characterize Co_3O_4-NC/NGr-12h after the stability test and the features are found to be same as they appeared before the stability test (Figure S8c,d, Supporting Information). The positions of the prominent peaks and distances between them are not changed after the stability test. This observation confirms the structural integrity after the potential cycling. Thus, the TEM and XPS data confirm that there is only negligible change in the morphology of Co_3O_4-NC/NGr-12h during the OER process. Collectively, the above data shows that the corrosion of NGr is insignificant in our Co_3O_4-NC/NGr-12h catalyst under the OER conditions designated above, even though we could not completely rule out the possibility of corrosion owing to the detection limits of the characterization techniques applied. We attribute the excellent stability of NGr to several properties. The graphitic carbon itself is chemically relatively inert and has been reported to be stable under oxidative environments.[17,41] Studies also have shown that corrosion of carbon when utilized as the catalyst substrates preferentially takes place at the

DOI: 10.1021/am506450c
ACS Appl. Mater. Interfaces 2015, 7, 442–451

amorphous carbon surface, defect sites and oxygen containing groups. Finally, the synergetic effect between Co_3O_4 and NGr also helps to prevent the carbon corrosion. Fast dissipation of the electrons generated from OER through the underlying NGr networks avoids the accumulation of electrons on NGr and subsequently the unwanted corrosion reactions. The optimal combination of the nanostructures also makes Co_3O_4-NC/NGr-12h a highly efficient catalyst with very low OER potentials, which in turn reduces the probability of carbon corrosion from occurring. In addition, the decrement of the current and increase in the overpotential encountered during 500 LSV cycle are mainly ascribed to the formation of primary and secondary passivation layers of Co(II) and Co(III), respectively on the electrode surface under the operating positive potential of 1.7 V vs RHE.[58,59] More clearly, as mentioned above, Co_3O_4-NC/NGr-12h has shown lower current decrement during the chronoamperometric stability test compared to the rest of the prepared samples and this could be credited to the presence of more stable and active low surface energy (blunt edge) planes in the system.

The Faradaic efficiency (ε) of Co_3O_4-NC/NGr-12h catalyst is determined by rotating-ring disk electrode (RRDE) investigation at 1600 rpm of the working electrode in 1 M KOH under N_2 atmosphere (detailed electrode preparation is given in the Supporting Information). This was measured by subjecting the disk electrode to a series of current steps from 0.2646 to 2.646 mA, holding the current for 1 min at each current steps and simultaneously keeping the ring at constant potential of 0.5 V (vs RHE). During the RRDE measurement, oxygen was produced at the disk electrode, which was collected and reduced at the Pt-ring electrode. Subsequently, the corresponding generated current from the ring-electrode was

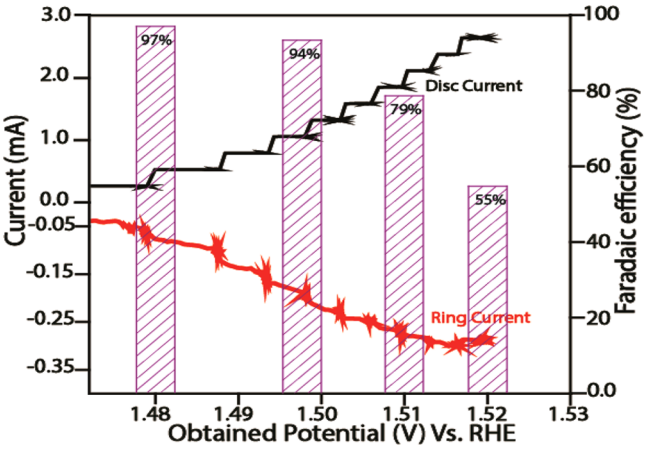

Figure 8. Rotating ring-disc electrode (RRDE) analysis of Co_3O_4-NC/NGr-12h sample showing the applied disc current, obtained ring current along with the Faradaic efficiency at different applied current steps.

measured (Figure 8). The Faradaic efficiency (ε) was calculated by using eq 1.[2]

$$\text{Faradaic efficiency } (\varepsilon) = 2 \times I_r/I_d \times N \quad (1)$$

where, I_r is the ring current, I_d is the disk current and N is the collection efficiency (0.37). Following this method, the measured value of ε is found to be ~97% at an applied current density of 1 mA cm^{-2}. The obtained Faradaic efficiency mainly describes the generation of oxygen at the disc and its simultaneous reduction at the Pt-ring.[2,60,61] The disk and ring currents of Co_3O_4-NC/NGr-12h catalyst in 1.0 M KOH are plotted as a function of the obtained disc potential in Figure 8. The obtained Faradaic efficiency (~97%) at an applied current density of 1 mA cm^{-2} (0.2646 mA) is found to be decreased to ~55% at 10 mA cm^{-2}. The decrease in the Faradaic efficiency with the applied current density could be ascribed to apparently undissolved oxygen bubbles generated at the relatively high applied disk current.[2] Most of the oxygen in the gas bubble cannot be collected by the Pt-ring electrode. The obtained higher faradaic efficiency at 1 mA cm^{-2} suggests that the disc current is mainly attributed to OER rather than the non-OER reactions (e.g., carbon corrosion). The obtained faradaic efficiency value is matching with the literature reports, which validates significant activity of Co_3O_4-NC/NGr-12 h toward OER.[2,61]

CONCLUSION

In summary, low surface energy plane exposed Co_3O_4 nanocubes dispersed on nitrogen-doped graphene (Co_3O_4-NC/NGr) have been synthesized by a simple hydrothermal method. The sample designated as Co_3O_4-NC/NGr-12h has shown the lowest overpotential (~280 mV) for OER at a practical current density of 10 mA cm^{-2}. Moreover, the chronoamperometric and voltammetric stability tests highlight better sustainability of Co_3O_4-NC/NGr-12h in alkaline medium compared to its counterparts. From the detailed structural and electrochemical investigations, it could be concluded that the presence of the exposed low surface energy crystal planes of Co_3O_4 nanocubes and their synergistic interaction between NGr in Co_3O_4-NC/NGr-12h are responsible for favorably tuning the properties of the electrocatalyst for OER. To the best of our knowledge, this is one of the promising results reported in the category of Co oxide supported on carbon materials for OER by exploring the surface plane and its energy. Moreover, Co_3O_4-NC/NGr is relatively cheap and it has an established excellent corrosion resistance property in aqueous alkaline systems. Hence, it offers an efficient and cheap alternative to the energy intensive and expensive RuO_2/IrO_2 systems.

ASSOCIATED CONTENT

Supporting Information

Electrochemical studies, histogram of Co_3O_4-NC particle size distribution on Gr and NGr, different planes of cubic crystal, thermogravimetric analysis, X-ray photoelectron spectra of C 1s of NGr, impedance analysis, cyclic voltammetry analysis of Co_3O_4-NC/NGr-12h, mass activity of the catalysts, TEM and XPS analysis of Co_3O_4-NC/NGr-12h, after durability test, Raman bands and I_D/I_G ratio of Gr and NGr supported catalysts, comparison of the overpotential values for the reported Co based electrocatalysts, reported overpotential values for the benchmark electrocatalysts, and overpotentials of NGr, Co_3O_4, Co_3O_4-NC/Gr-12h, Co_3O_4-NC/NGr-*X*h (X = 3, 9, 12, 24) catalysts. This material is available free of charge via the Internet at http://pubs.acs.org.

AUTHOR INFORMATION

Corresponding Author

*S. Kurungot. E-mail: k.sreekumar@ncl.res.in.

DOI: 10.1021/am506450c
ACS Appl. Mater. Interfaces 2015, 7, 442−451

Author Contributions

The paper was written through contributions of all authors. All authors have given approval to the final version of the paper.

Funding

This study was financially supported by Council of Scientific and Industrial Research (CSIR), New Delhi, India, by HYDEN project (CSC0122) funding to SK and research fellowship to S.K.S.

Notes

The authors declare no competing financial interest.

■ ACKNOWLEDGMENTS

S.K.S. greatly acknowledges the Council of Scientific and Industrial Research (CSIR), New Delhi, India, for a Junior Research Fellowship. Financial support of the CSIR through the HYDEN programme (CSC0122) is gratefully acknowledged.

■ REFERENCES

(1) Li, Y.; Gong, M.; Liang, Y.; Feng, J.; Kim, J.; Wang, H.; Hong, V.; Zhang, B.; Dai, H. Advanced Zinc-Air Batteries Based on High-Performance Hybrid Electrocatalysts. *Nat. Commun.* **2013**, *4*, 1805, DOI: 10.1038/ncomms2812.

(2) McCrory, C. C. L.; Jung, S.; Peters, J. C.; Jaramillo, T. F. Benchmarking Heterogeneous Electrocatalysts for the Oxygen Evolution Reaction. *J. Am. Chem. Soc.* **2013**, *135*, 16977−16987.

(3) Kim, J.; Yang, W.; Salim, J.; Ma, C.; Sun, C.; Li, J.; Kim, Y. Li-Water Battery with Oxygen Dissolved in Water as a Cathode. *J. Electrochem. Soc.* **2014**, *161*, A285−A289.

(4) Fang, Y. H.; Liu, Z. P. Mechanism and Tafel Lines of Electro-Oxidation of Water to Oxygen on RuO_2(110). *J. Am. Chem. Soc.* **2010**, *132*, 18214−18222.

(5) Louie, M. W.; Bell, A. T. An Investigation of Thin-Film Ni−Fe Oxide Catalysts for the Electrochemical Evolution of Oxygen. *J. Am. Chem. Soc.* **2013**, *135*, 12329−12337.

(6) Liang, Y.; Wang, H.; Zhou, J.; Li, Y.; Wang, J.; Regier, T.; Dai, H. Covalent Hybrid of Spinel Manganese−Cobalt Oxide and Graphene as Advanced Oxygen Reduction Electrocatalysts. *J. Am. Chem. Soc.* **2012**, *134*, 3517−3523.

(7) Chou, N. H.; Ross, P. N.; Bell, A. T.; Tilley, T. D. Comparison of Cobalt-based Nanoparticles as Electrocatalysts for Water Oxidation. *ChemSusChem* **2011**, *4*, 1566−1569.

(8) Lee, S. W.; Carlton, C.; Risch, M.; Surendranath, Y.; Chen, S.; Furutsuki, S.; Yamada, A.; Nocera, D. G.; Shao-Horn, Y. The Nature of Lithium Battery Materials under Oxygen Evolution Reaction Conditions. *J. Am. Chem. Soc.* **2012**, *134*, 16959−16962.

(9) Bajdich, M.; García, M. M.; Vojvodic, A.; Nørskov, J. K.; Bell, A. T. Theoretical Investigation of the Activity of Cobalt Oxides for the Electrochemical Oxidation of Water. *J. Am. Chem. Soc.* **2013**, *135*, 13521−13530.

(10) Lyon, M. E. G.; Brandon, M. P. The Oxygen Evolution Reaction on Passive Oxide Covered Transition Metal Electrodes in Aqueous Alkaline Solution. Part 1-Nickel. *Int. J. Electrochem. Sci.* **2008**, *3*, 1386−1424.

(11) Jung, J.; Jeong, H. Y.; Lee, J. S.; Kim, M. G.; Cho, A. Bifunctional Perovskite Catalyst for Oxygen Reduction and Evolution. *Angew. Chem., Int. Ed.* **2014**, *53*, 4582−4586.

(12) Yang, W.; Salim, J.; Li, S.; Sun, C.; Chen, L.; Goodenough, J. B.; Kim, Y. Perovskite $Sr_{0.95}Ce_{0.05}CoO_{3-\delta}$ Loaded with Copper Nanoparticles as a Bifunctional Catalyst for Lithium-Air Batteries. *J. Mater. Chem.* **2012**, *22*, 18902−18907.

(13) Maiyalagan, T.; Chemelewski, K. R.; Manthiram, A. Role of the Morphology and Surface Planes on the Catalytic Activity of Spinel $LiMn_{1.5}Ni_{0.5}O_4$ for Oxygen Evolution Reaction. *ACS Catal.* **2014**, *4*, 421−425.

(14) Duan, J.; Chen, S.; Dai, S.; Qiao, S. Z. Shape Control of Mn_3O_4 Nanoparticles on Nitrogen-Doped Graphene for Enhanced Oxygen Reduction Activity. *Adv. Funct. Mater.* **2014**, *24*, 2072−2078.

(15) Yang, W.; Salim, J.; Ma, C.; Ma, Z.; Sun, C.; Li, J.; Chen, L.; Kim, Y. Flowerlike Co_3O_4 Microspheres Loaded with Copper Nanoparticle as an Efficient Bifunctional Catalyst for Lithium−Air Batteries. *Electrochem. Commun.* **2013**, *28*, 13−16.

(16) Fu, C.; Zhao, G.; Zhang, H.; Li, S. Evaluation and Characterization of Reduced Graphene Oxide Nanosheets as Anode Materials for Lithium-Ion Batteries. *Int. J. Electrochem. Sci.* **2013**, *8*, 6269−6280.

(17) Zhao, Y.; Nakamura, R.; Kamiya, K.; Nakanishi, S.; Hashimoto, K. Nitrogen-Doped Carbon Nanomaterials as Non-metal Electrocatalysts for Water Oxidation. *Nat. Commun.* **2013**, *4*, 2390.

(18) Unni, S. M.; Devulapally, S.; Karjule, N.; Kurungot, S. Graphene Enriched with Pyrrolic Coordination of the Doped Nitrogen as an Efficient Metal-Free Electrocatalyst for Oxygen Reduction. *J. Mater. Chem.* **2012**, *22*, 23506−23513.

(19) Park, S.; An, J.; Potts, J. R.; Velamakanni, A.; Murali, S.; Ruoff, R. S. Hydrazine-Reduction of Graphite and Graphene Oxide. *Carbon* **2011**, *49*, 3019−3023.

(20) Tao, A. R.; Habas, S.; Yang, P. Shape Control of Colloidal Metal Nanocrystals. *Small* **2008**, *4*, 310−325.

(21) Pileni, M. The Role of Soft Colloidal Templates in Controlling the Size and Shape of Inorganic Nanocrystals. *Nat. Mater.* **2003**, *2*, 145−150.

(22) Liang, Y.; Wang, Y.; Li, H.; Zhou, J.; Wang, J.; Regier, T.; Dai, H. Co_3O_4 Nanocrystals on Graphene as a Synergistic Catalyst for Oxygen Reduction Reaction. *Nat. Mater.* **2011**, *10*, 780−786.

(23) Mao, S.; Wen, Z.; Huang, T.; Hou, Y.; Chen, J. High-Performance Bi-functional Electrocatalysts of 3D Crumpled Graphene−Cobalt Oxide Nanohybrids for Oxygen Reduction and Evolution Reactions. *Energy Environ. Sci.* **2014**, *7*, 609−616.

(24) Liang, Y.; Li, Y.; Wang, H.; Dai, H. Strongly Coupled Inorganic/Nanocarbon Hybrid Materials for Advanced Electrocatalysis. *J. Am. Chem. Soc.* **2013**, *135*, 2013−2036.

(25) Sun, C.; Li, F.; Ma, C.; Wang, Y.; Ren, Y.; Yang, W.; Ma, Z.; Li, J.; Chen, Y.; Kim, Y.; Chen, L. Graphene−Co_3O_4 Nanocomposite as an Efficient Bifunctional Catalyst for Lithium−Air Batteries. *J. Mater. Chem. A* **2014**, *2*, 7188−7196.

(26) Friebel, D.; Bajdich, M.; Yeo, B. S.; Louie, M. W.; Miller, D. J.; Casalongue, H. S.; Mbuga, F.; Weng, T.; Nordlund, D.; Sokaras, D.; Alonso-Mori, R.; Bell, A. T.; Nilsson, A. On the Chemical State of Co-Oxide Electrocatalysts During Alkaline Water Splitting. *Phys. Chem. Chem. Phys.* **2013**, *15*, 17460−17567.

(27) Wang, Z.; Xu, D.; Xu, J.; Zhang, X. Oxygen Electrocatalysts in Metal−Air Batteries: From Aqueous to Nonaqueous Electrolytes. *Chem. Soc. Rev.* **2014**, *43*, 7746−7786.

(28) Hamdani, M.; Singh, R. N.; Chartier, P. Co_3O_4 and Co-Based Spinel Oxides Bifunctional Oxygen Electrodes. *Int. J. Electrochem. Sci.* **2010**, *5*, 556−577.

(29) Wu, J.; Xue, Y.; Yan, X.; Yan, W.; Chen, Q.; Xie, Y. Co_3O_4 Nanocrystals on Single-Walled Carbon Nanotubes as a Highly Efficient Oxygen-Evolving Catalyst. *Nano Res.* **2012**, *5*, 521−530.

(30) Reier, T.; Oezaslan, M.; Strasser, P. Electrocatalytic Oxygen Evolution Reaction (OER) on Ru, Ir, and Pt Catalysts: A Comparative Study of Nanoparticles and Bulk Materials. *ACS Catal.* **2012**, *2*, 1765−1772.

(31) Marcano, D. C.; Kosynkin, D. V.; Berlin, J. M.; Sinitskii, A.; Sun, Z.; Slesarev, A.; Alemany, L. B.; Lu, W.; Tour, J. M. Improved Synthesis of Graphene Oxide. *ACS Nano* **2010**, *4*, 4806−4814.

(32) Li, W.; Geng, X.; Guo, Y.; Rong, J.; Gong, Y.; Wu, L.; Zhang, X.; Li, P.; Xu, J.; Cheng, G.; Sun, M.; Liu, L. Reduced Graphene Oxide Electrically Contacted Graphene Sensor for Highly Sensitive Nitric Oxide Detection. *ACS Nano* **2011**, *5*, 6955−6961.

(33) Sheng, Z.; Shao, L.; Chen, J.; Bao, W.; Wang, F.; Xia, X. Catalyst-Free Synthesis of Nitrogen-Doped Graphene *via* Thermal Annealing Graphite Oxide with Melamine and Its Excellent Electrocatalysis. *ACS Nano* **2011**, *5*, 4350−4358.

DOI: 10.1021/am506450c
ACS Appl. Mater. Interfaces 2015, 7, 442−451

(34) Chung, H. T.; Won, J. H.; Zelenay, P. Active and Stable Carbon Nanotube/Nanoparticle Composite Electrocatalyst for Oxygen Reduction. *Nat. Commun.* **2013**, *4*, DOI: 10.1038/ncomms2944.
(35) Xia, X.; Tu, J.; Zhang, Y.; Wang, X.; Gu, C.; Zhao, X.; Fan, H. J. High-Quality Metal Oxide Core/Shell Nanowire Arrays on Conductive Substrates for Electrochemical Energy Storage. *ACS Nano* **2012**, *6*, 5531−5538.
(36) Yang, J.; Liu, H.; Martens, W. N.; Frost, R. L. Synthesis and Characterization of Cobalt Hydroxide, Cobalt Oxyhydroxide, and Cobalt Oxide Nanodiscs. *J. Phys. Chem. C* **2010**, *114*, 111−119.
(37) Sa, Y. J.; Kwon, K.; Cheon, J. Y.; Kleitzc, F.; Joo, S. H. Ordered Mesoporous Co_3O_4 Spinels as Stable, Bi-functional, Noble Metal-Free Oxygen Electrocatalysts. *J. Mater. Chem. A* **2013**, *1*, 9992−10001.
(38) Wu, G.; Mack, N. H.; Gao, W.; Ma, S.; Zhong, R.; Han, J.; Baldwin, J. K.; Zelenay, P. Nitrogen-Doped Graphene-Rich Catalysts Derived from Heteroatom Polymers for Oxygen Reduction in Nonaqueous Lithium O_2 Battery Cathodes. *ACS Nano* **2012**, *6*, 9764−9776.
(39) Han, J.; Kim, H.; Kim, D. Y.; Jo, S. M.; Jang, S. Water-Soluble Polyelectrolyte-Grafted Multiwalled Carbon Nanotube Thin Films for Efficient Counter Electrode of Dye-Sensitized Solar Cells. *ACS Nano* **2010**, *4*, 3503−3509.
(40) Palaniselvam, T.; Kannan, R.; Kurungot, S. Facile Construction of Non-precious Iron Nitride-Doped Carbon Nanofibers as Cathode Electrocatalysts for Proton Exchange Membrane Fuel Cells. *Chem. Commun.* **2011**, *47*, 2910−2912.
(41) Palaniselvam, T.; Irshad, A.; Unni, B.; Kurungot, S. Activity Modulated Low Platium Content Oxygen Reduction Electrocatalysts Prepared by Inducing Nano-Order Dislocations on Carbon Nanofiber through N_2-Doping. *J. Phys. Chem. C* **2012**, *116*, 14754−14763.
(42) Dhavale, V. M.; Gaikwad, S. S.; Kurungot, S. Activated Nitrogen Doped Graphene Shell Towards Electrochemical Oxygen Reduction Reaction by its Encapsulation on Au Nanoparticle (Au@N-Gr) in Water-in-Oil "Nanoreactors". *J. Mater. Chem. A* **2014**, *2*, 1383−1390.
(43) Ziegelbauer, J. M.; Olson, T. S.; Pylypenko, S.; Alamgir, F.; Jaye, C.; Atanassov, P.; Mukerjee, S. Direct Spectroscopic Observation of the Structural Origin of Peroxide Generation from Co-Based Pyrolyzed Porphyrins for ORR Applications. *J. Phys. Chem. C* **2008**, *112*, 8839−8849.
(44) Artyushkova, K.; Pylypenko, S.; Olson, T. S.; Fulghum, J. E.; Atanassov, P. Predictive Modeling of Electrocatalyst Structure Based on Structure-to-Property Correlations of X-ray Photoelectron Spectroscopic and Electrochemical Measurements. *Langmuir* **2008**, *24*, 9082−9088.
(45) Zafeiratos, S.; Dintzer, T.; Teschner, D.; Blume, R.; Hävecker, M.; Knop-Gericke, A.; Schlögl, R. Methanol Oxidation Over Model Cobalt Catalysts: Influence of the Cobalt Oxidation State on the Reactivity. *J. Catal.* **2010**, *269*, 309−317.
(46) Yang, H. T.; Su, Y. K.; Shen, C. M.; Yang, T. Z.; Gao, H. J. Synthesis and Magnetic Properties of ε-Cobalt Nanoparticles. *Surf. Interface Anal.* **2004**, *36*, 155−160.
(47) Baddour-Hadjean, R.; Pereira-Ramos, J. Raman Microspectrometry Applied to the Study of Electrode Materials for Lithium Batteries. *Chem. Rev.* **2010**, *110*, 1278−1319.
(48) Palaniselvam, T.; Valappil, M. O.; Illathvalappil, R.; Kurungot, S. Nanoporous Graphene by Quantum Dots Removal from Graphene and its Conversion to a Potential Oxygen Reduction Electrocatalyst via Nitrogen Doping. *Energy Environ. Sci.* **2014**, *7*, 1059−1067.
(49) Li, G.; Yu, H.; Wang, X.; Sun, S.; Li, Y.; Shao, Z.; Yi, B. Highly Effective $Ir_xSn_{1-x}O_2$ Electrocatalysts for Oxygen Evolution Reaction in the Solid Polymer Electrolyte Water Electrolyser. *Phys. Chem. Chem. Phys.* **2013**, *15*, 2858−2866.
(50) Chen, Z.; Higgins, D.; Yu, A.; Zhang, L.; Zhang, J. A Review on Non-precious Metal Electrocatalysts for PEM Fuel Cells. *Energy Environ. Sci.* **2011**, *4*, 3167−3192.
(51) Petitto, S. C.; Marsh, E. M.; Carson, G. A.; Langell, M. A. Cobalt Oxide Surface Chemistry: The Interaction of CoO(100), Co_3O_4(110), and Co_3O_4(111) with Oxygen and Water. *J. Mol. Catal. A: Chem.* **2008**, *281*, 49−58.
(52) Wei, G.; Fang, Y.; Liu, Z. First Principles Tafel Kinetics for Resolving Key Parameters in Optimizing Oxygen Electrocatalytic Reduction Catalyst. *J. Phys. Chem. C* **2012**, *116*, 12696−12705.
(53) Tomas-Garcia, A. L.; Li, Q.; Oluf, J.; Jensen; Bjerrum, N. J. High Surface Area Tungsten Carbides: Synthesis, Characterization and Catalytic Activity towards the Hydrogen Evolution Reaction in Phosphoric Acid at Elevated Temperatures. *Int. J. Electrochem. Sci.* **2014**, *9*, 1016−1032.
(54) Kong, D.; Wang, H.; Lu, Z.; Cui, Y. $CoSe_2$ Nanoparticles Grown on Carbon Fiber Paper: An Efficient and Stable Electrocatalyst for Hydrogen Evolution Reaction. *J. Am. Chem. Soc.* **2014**, *136*, 4897−4900.
(55) Nakagawa, T.; Beasley, C. A.; Murray, R. W. Efficient Electro-Oxidation of Water Near its Reversible Potential by a Mesoporous IrOx Nanoparticle Film. *J. Phys. Chem. C* **2009**, *113*, 12958−12961.
(56) Wang, X. X.; Tan, Z. H.; Zeng, M.; Wang, J. N. Carbon Nanocages: A New Support Material for Pt Catalyst with Remarkably High Durability. *Sci. Rep.* **2013**, *4*, 1−11.
(57) Khun, N. W.; Liu, E. Nitrogen-Induced Degradation of Corrosion Resistance of Platinum/Ruthenium/Nitrogen-Doped Diamond-like Carbon Thin Films. *J. Electrochem. Soc.* **2010**, *157*, C269−C274.
(58) Foelske, A.; Strehblow, H. Passivity of Cobalt in Borate Buffer at pH 9.3 Studied by X-ray Photoelectron Spectroscopy. *Surf. Interface Anal.* **2000**, *29*, 548−555.
(59) Lin, F.; Nordlund, D.; Pan, T.; Markus, I. M.; Weng, T.; Xin, H. L.; Doeff, M. M. Influence of Synthesis Conditions on the Surface Passivation and Electrochemical Behavior of Layered Cathode Materials. *J. Mater. Chem. A* **2014**, *2*, 19833−19840.
(60) Suntivich, J.; May, K. J.; Gasteiger, H. A.; Goodenough, J. B.; Shao-Horn, Y. A Perovskite Oxide Optimized for Oxygen Evolution Catalysis from Molecular Orbital Principles. *Science* **2011**, *334*, 1383−1385.
(61) Qiu, Y.; Xin, L.; Li, W. Electrocatalytic Oxygen Evolution over Supported Small Amorphous Ni−Fe Nanoparticles in Alkaline Electrolyte. *Langmuir* **2014**, *30*, 7893−7901.
(62) Ryu, W.; Yoon, T.; Song, S. H.; Jeon, S.; Park, Y.; Kim, I. Bifunctional Composite Catalysts Using Co_3O_4Nanofibers Immobilized on Nonoxidized Graphene Nanoflakes for High-Capacity and Long-Cycle Li−O_2 Batteries. *Nano Lett.* **2013**, *13*, 4190−4197.
(63) Xiao, J.; Kuang, Q.; Yang, S.; Xiao, F.; Wang, S.; Guo, L. Surface Structure Dependent Electrocatalytic Activity of Co_3O_4 Anchored on Graphene Sheets toward Oxygen Reduction Reaction. *Sci. Rep.* **2013**, *3*, DOI: 10.1038/srep02300.
(64) Hong, S.; Shin, Y. H.; Ihm, J. Crystal Shape of a Nickel Particle Related to Carbon Nanotube Growth. *Jpn. J. Appl. Phys.* **2002**, *41*, 6142−6144.
(65) Dhavale, V. M.; Gaikwad, S. S.; George, L.; Devi, R. N.; Kurungot, S. Nitrogen-Doped Graphene Interpenetrated 3D Ni-Nanocages: Efficient and Stable Water-to-Dioxygen Electrocatalysts. *Nanoscale* **2014**, *6*, 13179−13187.
(66) Yu, K.; Lu, G.; Bo, Z.; Mao, S.; Chen, J. Carbon Nanotube with Chemically Bonded Graphene Leaves for Electronic and Optoelectronic Applications. *J. Phys. Chem. Lett.* **2011**, *2*, 1556−1562.

DOI: 10.1021/am506450c
ACS Appl. Mater. Interfaces 2015, 7, 442−451